

Supplement of Atmos. Chem. Phys., 20, 15427–15442, 2020  
<https://doi.org/10.5194/acp-20-15427-2020-supplement>  
© Author(s) 2020. This work is distributed under  
the Creative Commons Attribution 4.0 License.



*Supplement of*

## **Measurement report: Source and mixing state of black carbon aerosol in the North China Plain: implications for radiative effect**

**Qiyuan Wang et al.**

*Correspondence to:* Qiyuan Wang (wangqy@ieecas.cn) and Junji Cao (cao@loess.llqg.ac.cn)

The copyright of individual parts of the supplement might differ from the CC BY 4.0 License.

28 **Section S1. Complementary measurements**

29 Daily PM<sub>2.5</sub> Teflon<sup>®</sup> filters (Whatman Limited, Maidstone, UK) and quartz-fiber filters  
30 (QM/A; GE Healthcare, Chicago, IL, USA) were collected simultaneously from 09:00  
31 local time to 09:00 the next day using a mini-volume sampler (Airmetrics, Oregon, USA)  
32 and a high-volume air sampler (Tisch Environmental, Inc., USA), respectively. The  
33 sampled filters were stored in a refrigerator at 4°C to minimize the evaporation of volatile  
34 materials before chemical analyses. The Teflon<sup>®</sup> filters were used in the determination of  
35 inorganic elements while the quartz-fiber filters were used in the analysis of carbonaceous  
36 matter and water-soluble inorganic ions. Field blanks were also collected and analysed to  
37 minimize the possible background artifact.

38 The elements were analysed by an Energy-Dispersive X-ray Fluorescence (ED-XRF)  
39 spectrometry (Epsilon 5 ED-XRF, PANalytical B.V., Netherlands). Detailed description of  
40 the ED-XRF was done by in Xu et al. (2012). Organic carbon (OC) and elemental carbon  
41 (EC) were determined by a thermal/optical carbon analyzer (Desert Research Institute  
42 Model 2001, Atmoslytic Inc., Calabasa, CA, USA). Detailed analytical procedures were  
43 described by Cao et al. (2003). Cations (i.e., NH<sub>4</sub><sup>+</sup>, K<sup>+</sup>, Mg<sup>2+</sup>, Ca<sup>2+</sup>) and anions (i.e., F<sup>-</sup>, Cl<sup>-</sup>,  
44 NO<sub>3</sub><sup>-</sup>, and SO<sub>4</sub><sup>2-</sup>) were measured using a Dionex 600 Ion Chromatograph (IC, Dionex Corp.,  
45 Sunnyvale, CA, USA). A detailed description of the IC approach was done by Zhang et al.  
46 (2011).

47 Hourly wind speed, wind direction, temperature, and relative humidity were measured  
48 using an automatic weather station installed at the Xianghe Atmospheric Observatory. The  
49 hourly height of planetary boundary layer was retrieved from the Hybrid Single-Particle  
50 Lagrangian Integrated Trajectory (HYSPLIT) model (Draxler and Rolph, 2003). The  
51 mixing ratio of ozone (O<sub>3</sub>) was measured using an ultraviolet photometric Model 49i O<sub>3</sub>  
52 analyzer (Thermo Fisher Scientific, San Jose, CA, USA). It was calibrated using a standard  
53 reference gas of O<sub>3</sub> before and during the campaign.

54 **Section S2. Configuration of Weather Research and Forecasting model coupled**  
55 **with chemistry (WRF-Chem)**

56 The model resolution was 3 km × 3 km, and there were 300 grids in each of the latitude  
57 and longitude. The domain was concentrated in the North China Plain and the north of

58 Hebei Province, with the central location at 39.00°N, 117.00°E. There were thirty-five  
59 vertical layers from the Earth's surface up to 50 hPa. The horizontal grid projection is  
60 Lambert. The meteorological fields were retrieved from the National Centers for  
61 Environmental Prediction (NCEP) reanalysis data, with a spatial and temporal resolution  
62 of 1° × 1° and 6 h, respectively (<http://rda.ucar.edu/datasets/ds083.2>). The initial and lateral  
63 boundary conditions of black carbon (BC) were retrieved by 6 h output of the Model for  
64 Ozone and Related chemical Tracers, version 4 (MOZART-4, Emmons et al., 2010). A  
65 detailed description of configurations in WRF-Chem model used in this study are  
66 summarized in Table S3. The BC emission inventory with a spatial resolution of 0.25° ×  
67 0.25° included industry, power, transportation, and residential sources (e.g., fossil fuel and  
68 biofuel), which were based on the Multi-resolution Emission Inventory for China (MEIC)  
69 for the year of 2012 ([www.meicmodel.org](http://www.meicmodel.org)).

### 70 **Section S3. Optical Properties of Aerosols and Clouds (OPAC) model**

71 The aerosol optical depth (AOD), single scattering albedo (SSA), and asymmetric  
72 parameter (AP) are important parameters used in the SBDART model to estimate aerosol  
73 radiative effect. In this study, these optical parameters were derived by the OPAC model.  
74 A detailed description of the software package of OPAC has been documented by Hess et  
75 al. (1998). The measured mass concentrations of OC, EC, and water-soluble ions as well  
76 as the estimated mineral dust (= [Fe]/0.035) were input in the OPAC model to estimate the  
77 AOD, SSA, and AP. The measurements of these chemical species are described in Text S1.  
78 The number concentration of BC in the OPAC model was constrained by the measured EC  
79 mass concentration. Although several water-soluble ions and mineral dust were obtained,  
80 they did not cover all water-soluble and insoluble materials. Therefore, the number  
81 concentrations of water-soluble and insoluble materials were tuned for OPAC model based  
82 on the measured data. This was done by comparing the OPAC-derived light scattering,  
83 light absorption, and SSA with the corresponding PAX-measured ones until the differences  
84 were within 5% for each parameter. After the aerosol light extinction coefficient (sum of  
85 light scattering and absorption) was obtained, the AOD was then estimated as follows (Hess  
86 et al., 1998):

$$87 \quad \text{AOD} = \sum_j \int_{H_{j,\min}}^{H_{j,\max}} \sigma_{e,j}(h) dh = \sum_j \sigma_{e,j}^1 N_j(0) \int_{H_{j,\min}}^{H_{j,\max}} e^{-\frac{h}{z_j}} dh \quad (\text{S1})$$

88 where  $H_{j,max}$  and  $H_{j,min}$  were the upper and lower boundary in layer  $j$ ;  $\sigma_{e,j}$  was the surface  
89 aerosol light extinction coefficient in layer  $j$ ;  $h$  was the layer height;  $\sigma_{e,j}^1$  represented the  
90 aerosol light extinction coefficient that was normalized to 1 particle  $\text{cm}^{-3}$ ;  $N_j$  was the  
91 number concentration in layer  $j$ ; and  $Z$  was the scale height. The OPAC-derived AODs  
92 were tuned to match the satellite-derived AODs (<https://giovanni.gsfc.nasa.gov/giovanni>)  
93 by altering the scale height in OPAC until the difference between them was within 5%.  
94 Owing to the closure with AOD and anchoring of the chemical composition, the  
95 assumptions in the OPAC model did not exhibit a significant impact on the estimation of  
96 radiative effect using SBDART model (Satheesh and Srinivasan 2006).  
97

**Table S1.** Summary of the mass concentrations of black carbon (BC) and its contribution from different sources in China and other countries.

Region	Site type	Site	Period	<sup>a</sup> Method	<sup>b</sup> BC <sub>lff</sub> (%)	<sup>c</sup> BC <sub>sf</sub> (%)	<sup>d</sup> BC <sub>ff</sub> (%)	<sup>e</sup> BC <sub>bb</sub> (%)	Reference
China	Urban	Beijing	winter, 2015	aeth. mode	30	70			Liu et al., 2018
		Beijing	winter, 2013	$\Delta^{14}\text{C}$	8	92			Andersson et al., 2015
		Beijing-Tianjin-Hebei	winter 2012	$\Delta^{14}\text{C}$	12	88			Yu et al., 2018
		Shanghai	winter, 2013	$\Delta^{14}\text{C}$	46	54			Andersson et al., 2015
		Guangzhou	winter, 2013	$\Delta^{14}\text{C}$	58	42			Andersson et al., 2015
	Suburban	Xianghe	winter, 2017	aeth. mode	69	31			This study
		Nanjing	winter, 2016	aeth. mode	84	16			Jing et al., 2019
Europe	Urban	Grenoble, France	winter	aeth. mode			82	18	Favez et al., 2010
		Paris, France	winter	aeth. mode			76	24	Crippa et al., 2013
		Madrid, Spain	winter	aeth. mode			93	7	Becerril-Valle et al., 2017
		Madrid, Spain	winter	aeth. mode			84	16	Becerril-Valle et al., 2017
		London, UK	winter	aeth. mode			77	23	Fuller et al., 2014
		Zurich, Switzerland	winter	aeth. mode			76	24	Herich et al., 2011
	Suburban	Paris, France	winter	aeth. mode			80	20	Crippa et al., 2013
		London, UK	winter	aeth. mode			85	15	Crilley et al., 2015
		Demokritos, Greece	winter	aeth. mode			67	33	Kalogridis et al., 2018
		Thiseio, Greece	winter	aeth. mode			71	29	Kalogridis et al., 2018

		Detling, Kent, England	winter	aeth. mode	70	30	Crilley et al., 2015
		Andalusia, Spain	winter	aeth. mode	12	88	Becerril-Valle et al., 2017
	Rural	Magadino-Cadenazzo, Swiss	winter	aeth. mode	70	30	Herich et al., 2011
		Payerne, Switzerland	winter	aeth. mode	67	33	Herich et al., 2011
		Swiss	winter	aeth. mode	49	51	Sandradewi et al., 2008
		Vavihill, Sweden	winter	aeth. mode	44	56	Martinsson et al., 2017
		Delhi, India	winter	aeth. mode	72	28	Dumka et al., 2018
South Asia	Urban	Ahmedabad, India	winter	aeth. mode	77	23	Rajesh and Ramachandran, 2017
		Gorakhpur, India	winter	aeth. mode	74	26	Vaishya et al., 2017
		IITM-Pashan, India	winter	aeth. mode	85	15	Kolhe et al., 2019

<sup>a</sup>aeth. mode represents aethalometer model.

<sup>b-e</sup>BC<sub>lff</sub>, BC<sub>sf</sub>, BC<sub>ff</sub>, and BC<sub>bb</sub> describe BC from liquid fossil fuel source, solid fuel source, fossil fuel source, and biomass burning, respectively.

**Table S2.** Descriptions of six different black carbon (BC) source regions in the case study from the Weather Research and Forecasting model coupled with chemistry (WRF-Chem).

Source Region	Location(s) of BC sources
Region 1	Xianghe
Region 2	Beijing
Region 3	Tianjin
Region 4	North China Plain (including south Hebei Province, northwest Shandong Province)
Region 5	North Hebei Province
Region 6	Other areas that not included in Region 1 – 5

**Table S3.** Summary of the configurations of Weather Research and Forecasting model coupled with chemistry (WRF-Chem).

Configuration	Description
Region	The North China Plain and north of Hebei Province
Simulation period	2-14 January 2018
Domain size	300 × 300
Domain center	39.00°N, 117.00°E
Horizontal resolution	3 km × 3 km
Vertical resolution	Thirty-five vertical layers from the Earth's surface up to 50 hPa
Microphysics scheme	WSM 5-classes microphysics scheme (Hong and Lim, 2006)
Boundary layer scheme	YSU PBL scheme (Hong et al., 2006)
Surface layer scheme	MM5 similarity (Zhang and Anthes, 1982)
Land-surface scheme	Noah land-surface model (Chen and Dudhia, 2001)
Longwave radiation scheme	RRTM scheme (Mlawer et al., 1997)
Shortwave radiation scheme	MM5 shortwave scheme (Dudhia, 1989)
Meteorological boundary and initial conditions	NCEP 1° × 1° reanalysis data
Chemical boundary and initial conditions	MOZART 6-h output (Emmons et al., 2010)
Anthropogenic emission inventory	industry, power, transportation, and residential sources (e.g., fossil fuel and biofuel)

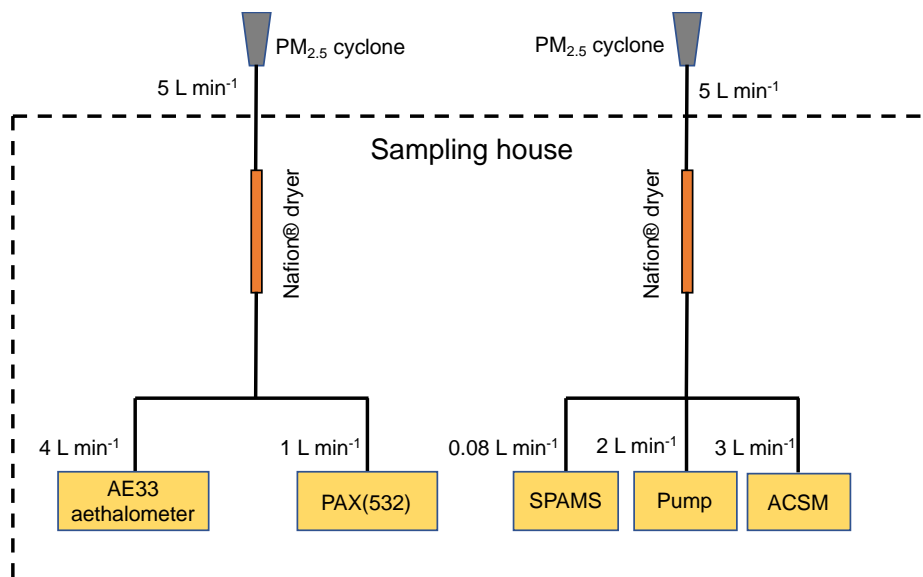


**Figure S1.** Schematic presentation of the instrumental setups of the ambient aerosol measurements.

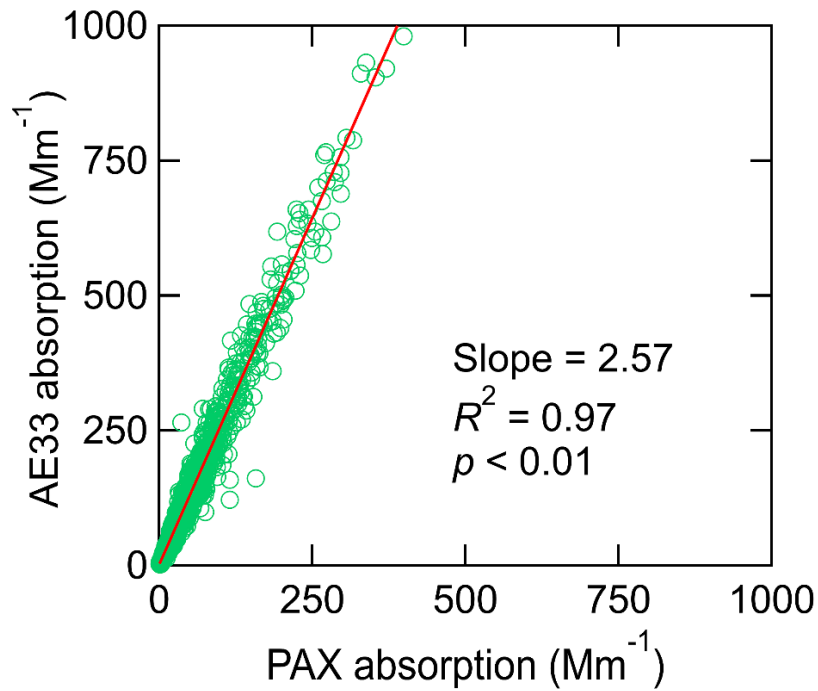


**Figure S2.** Relationship between the light absorption coefficients measured with AE33 aethalometer at a wavelength of 520 nm and photoacoustic extinctions (PAX) at a wavelength of 532 nm.

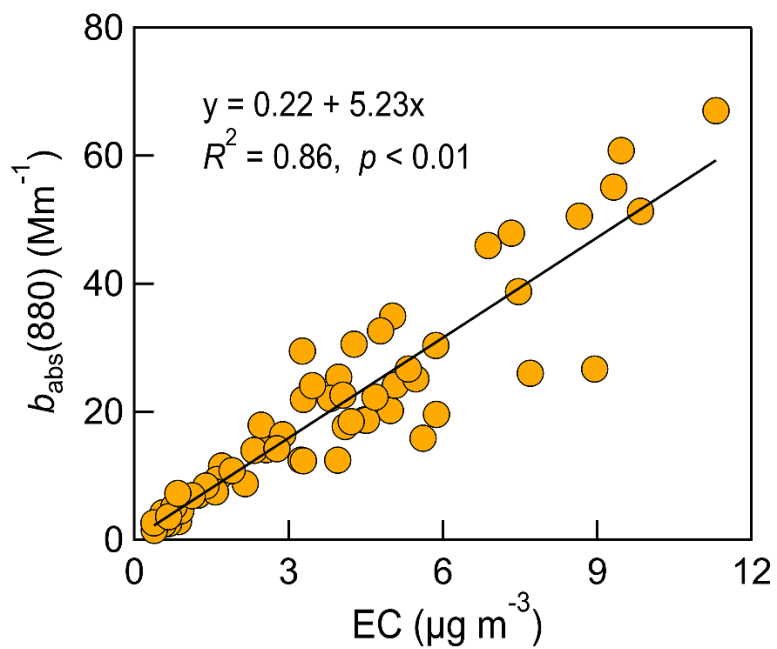


**Figure S3.** Relationship between the light absorption measured by AE33 aethalometer at a wavelength of 880 nm ( $b_{\text{abs}}(880)$ ) and the mass concentration of elemental carbon (EC).

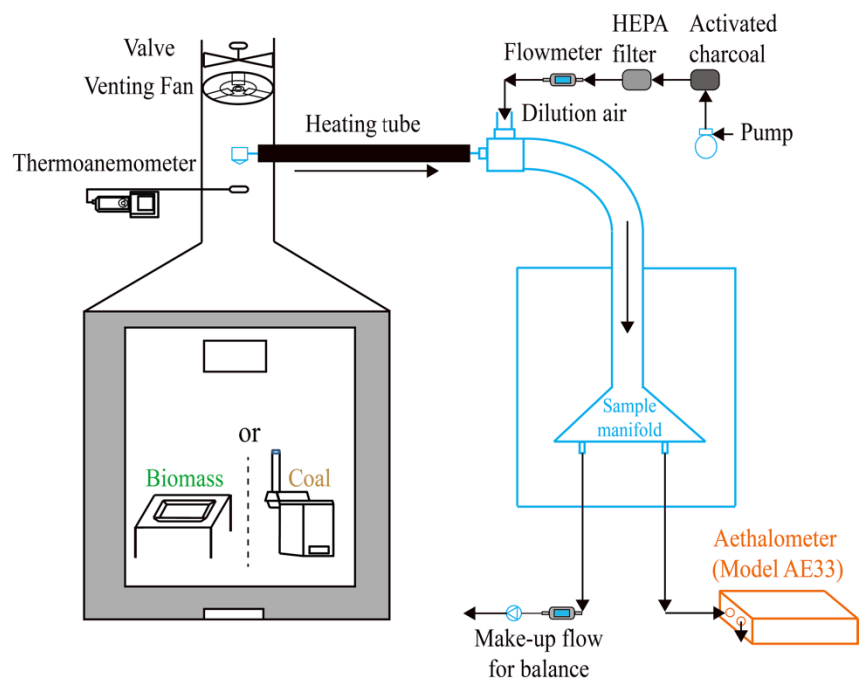


**Figure S4.** Schematic presentation of the instrumental setups of source experiments of biomass burning and coal combustion.

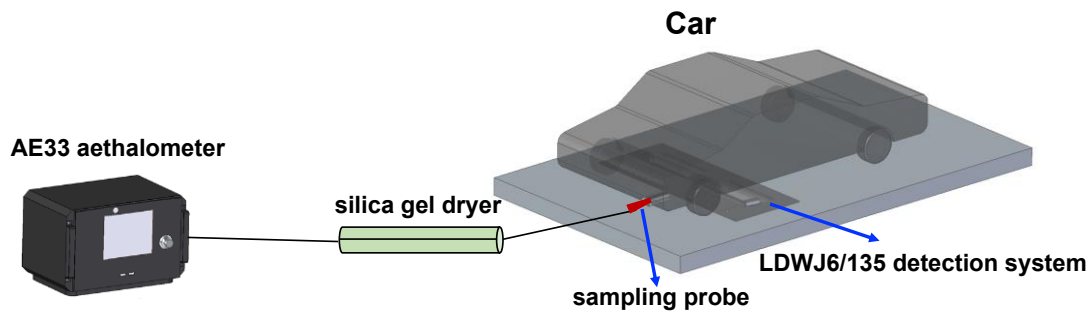


**Figure S5.** Schematic presentation of the instrumental setups of source experiment of vehicle emissions.

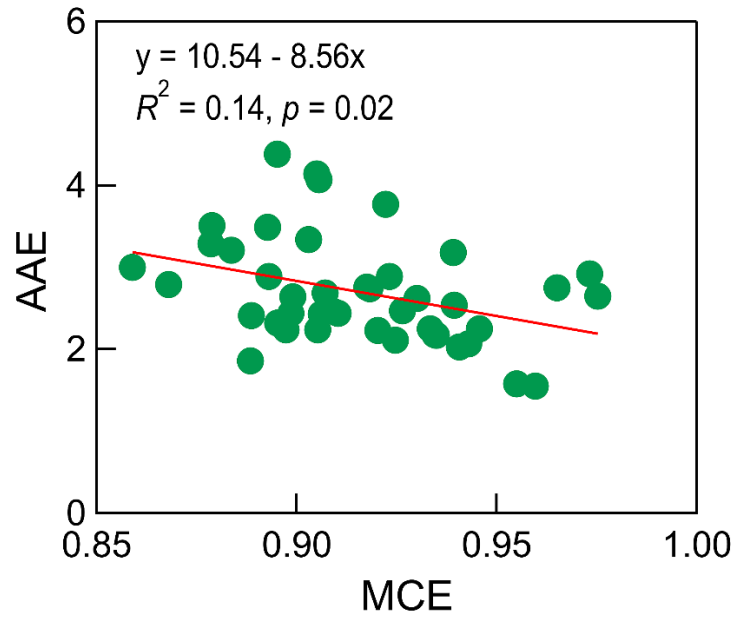


**Figure S6.** Scatter plot of aerosol absorption Ångström exponent (AAE) and modified combustion efficiency (MCE) from emissions of solid fuels. The MCE was calculated with carbon dioxide and carbon monoxide.

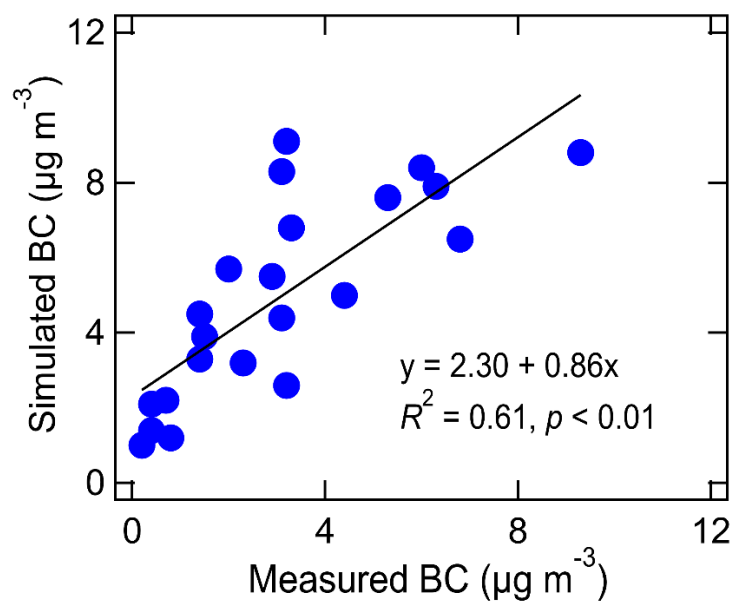


**Figure S7.** Relationship between the simulated and measured black carbon (BC) from 2nd to 23rd January, 2018. The simulated BC was determined using the Weather Research and Forecasting model coupled with chemistry (WRF-Chem).

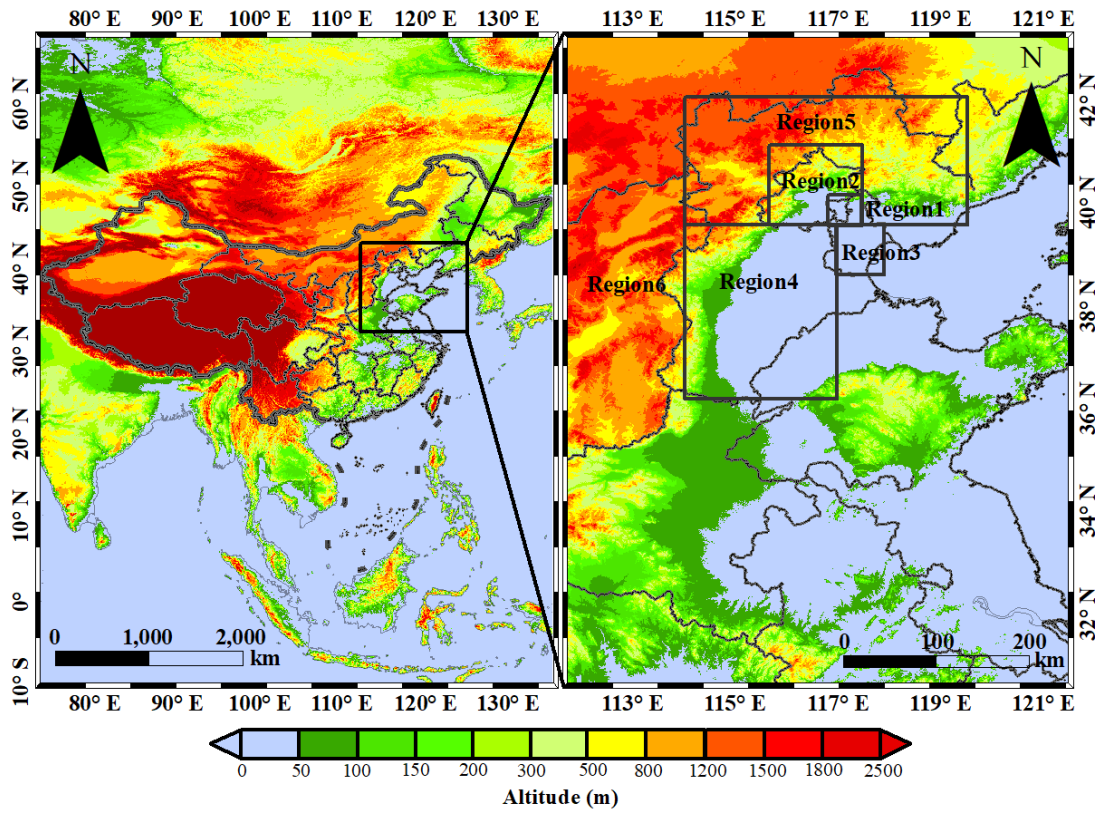


**Figure S8.** Division of different regions in the Weather Research and Forecasting model coupled with chemistry (WRF-Chem).

## References:

- Andersson, A., J. Deng, K. Du, M. Zheng, C. Yan, M. Sköld, & Ö. Gustafsson (2015). Regionally-varying combustion sources of the January 2013 severe haze events over eastern China. *Environmental Science & Technology*, 49(4), 2038–2043. <https://doi.org/10.1021/es503855e>
- Becerril-Valle, M., Coz, E., Prévôt, A. S. H., Močnik, G., Pandis, S. N., Sánchez de la Campa, A. M., et al. (2017). Characterization of atmospheric black carbon and co-pollutants in urban and rural areas of Spain. *Atmospheric Environment*, 169, 36–53. <https://doi.org/10.1016/j.atmosenv.2017.09.014>
- Cao, J. J., Lee, S. C., Ho, K. F., Zhang, X. Y., Zou, S. C., Fung, K., Chow, J. C., and Watson, J. G.: Characteristics of carbonaceous aerosol in Pearl River Delta Region, China during 2001 winter period, *Atmos. Environ.*, 37, 1451–1460, [https://doi.org/10.1016/S1352-2310\(02\)01002-6](https://doi.org/10.1016/S1352-2310(02)01002-6), 2003.
- Chen, F., & Dudhia, J. (2001). Coupling an advanced land surface-hydrology model with the Penn State-NCAR MM5 modeling system. Part I: Model implementation and sensitivity. *Monthly Weather Review*, 129, 569–585. [https://doi.org/10.1175/1520-0493\(2001\)129<0569:Caalsh>2.0.Co;2](https://doi.org/10.1175/1520-0493(2001)129<0569:Caalsh>2.0.Co;2)
- Crilly, L. R., Bloss, W. J., Yin, J., Beddows, D. C. S., Harrison, R. M., Allan, J. D., et al. (2015), Sources and contributions of wood smoke during winter in London: assessing local and regional influences. *Atmospheric Chemistry and Physics*, 15(6), 3149–3171. <https://doi.org/10.5194/acp-15-3149-2015>
- Crippa, M., DeCarlo, P. F., Slowik, J. G., Mohr, C., Heringa, M. F., Chirico, R., et al. (2013). Wintertime aerosol chemical composition and source apportionment of the organic fraction in the metropolitan area of Paris. *Atmospheric Chemistry and Physics*, 13(2), 961–981. <https://doi.org/10.5194/acp-13-961-2013>
- Draxler, R. R., and Rolph, G. D.: HYSPLIT (HYbrid Single-Particle Lagrangian Integrated Trajectory), Silver Spring, MD, Model access via NOAA ARL READY Website, available at: <https://ready.arl.noaa.gov/HYSPLIT.php> (last access: August 2019), 2003.
- Dudhia, J. (1989). Numerical study of convection observed during the winter monsoon experiment using a mesoscale two-dimensional model. *Journal of the Atmospheric*

*Sciences*, 46, 3077–3107. [https://doi.org/10.1175/1520-0469\(1989\)046<3077:Nsocod>2.0.Co;2](https://doi.org/10.1175/1520-0469(1989)046<3077:Nsocod>2.0.Co;2)

- Dumka, U. C., Kaskaoutis, D. G., Tiwari, S., Safai, P. D., Attri, S. D., Soni, V. K., et al. (2018). Assessment of biomass burning and fossil fuel contribution to black carbon concentrations in Delhi during winter. *Atmospheric Environment*, 194, 93–109. <https://doi.org/10.1016/j.atmosenv.2018.09.033>
- Emmons, L. K., Walters, S., Hess, P. G., Lamarque, J. F., Pfister, G. G., Fillmore, D., et al., (2010). Description and evaluation of the Model for Ozone and Related chemical Tracers, version 4 (MOZART-4). *Geoscientific Model Development*, 3, 43–67. <https://doi.org/10.5194/gmd-3-43-2010>, 2010
- Favez, O., El Haddad, I., Piot, C., Boréave, A., Abidi, E., Marchand, N., et al. (2010). Inter-comparison of source apportionment models for the estimation of wood burning aerosols during wintertime in an Alpine city (Grenoble, France). *Atmospheric Chemistry and Physics*, 10(12), 5295–5314. <https://doi.org/doi:10.5194/acp-10-5295-2010>
- Fuller, G. W., Tremper, A. H., Baker, T. D., Yttri, K. E., & Butterfield, D. (2014). Contribution of wood burning to PM<sub>10</sub> in London. *Atmospheric Environment*, 87, 87–94. <https://doi.org/10.1016/j.atmosenv.2013.12.037>
- Hess, M., Koepke, P., and Schult, I.: Optical properties of aerosols and clouds: The software package OPAC, *Bull. Amer. Meteorol. Soc.*, 79, 831–844, [https://doi.org/10.1175/1520-0477\(1998\)079<0831:Opoaac>2.0.Co;2](https://doi.org/10.1175/1520-0477(1998)079<0831:Opoaac>2.0.Co;2), 1998.
- Herich, H., Hueglin, C., & Buchmann, B. (2011). A 2.5 year's source apportionment study of black carbon from wood burning and fossil fuel combustion at urban and rural sites in Switzerland. *Atmospheric Measurement Techniques*, 4(7), 1409–1420. <https://doi.org/10.5194/amt-4-1409-2011>
- Hong, S.-Y., & Lim, J.-O. J. (2006). The WRF single-moment 6-class microphysics scheme (WSM6). *Journal of the Korean Meteorological Society*, 42, 129–151.
- Hong, S.-Y., Noh, Y., & Dudhia, J. (2006). A new vertical diffusion package with an explicit treatment of entrainment processes. *Monthly Weather Review*, 134, 2318–2341. <https://doi.org/10.1175/mwr3199.1>

- Jing, A., Zhu, B., Wang, H., Yu, X., An, J., & Kang H. (2019). Source apportionment of black carbon in different seasons in the northern suburb of Nanjing, China. *Atmospheric Environment*, 201, 190–200. <https://doi.org/10.1016/j.atmosenv.2018.12.060>
- Kalogridis, A. C., Vratolis, S., Liakakou, E., Gerasopoulos, E., Mihalopoulos, N., & Eleftheriadis, K. (2018). Assessment of wood burning versus fossil fuel contribution to wintertime black carbon and carbon monoxide concentrations in Athens, Greece. *Atmospheric Chemistry and Physics*, 18(14), 10219–10236. <https://doi.org/10.5194/acp-18-10219-2018>
- Kolhe, A. R., Ralegankar, S. D., Safai, P. D., & Aher, G. R. (2019). Absorption properties of black carbon aerosols over environmentally distinct locations in south-western India: Temporal, spectral characterization and source apportionment. *Journal of Atmospheric and Solar-Terrestrial Physics*, 189, 1–17. <https://doi.org/10.1016/j.jastp.2019.03.010>
- Liu, Y., Yan, C., & Zheng, M. (2018). Source apportionment of black carbon during winter in Beijing. *Science of The Total Environment*, 618, 531–541. <https://doi.org/10.1016/j.scitotenv.2017.11.053>
- Martinsson, J., Abdul Azeem, H., Sporre, M. K., Bergström, R., Ahlberg, E., Öström, E., et al., A. (2017). Carbonaceous aerosol source apportionment using the Aethalometer model – evaluation by radiocarbon and levoglucosan analysis at a rural background site in southern Sweden. *Atmospheric Chemistry and Physics*, 17(6), 4265–4281. <https://doi.org/10.5194/acp-17-4265-2017>
- Mlawer, E. J., Taubman, S. J., Brown, P. D., Iacono, M. J., & Clough, S. A. (1997). Radiative transfer for inhomogeneous atmospheres: RRTM, a validated correlated-k model for the longwave. *Journal of Geophysical Research-Atmospheres*, 102, 16663–16682. <https://doi.org/10.1029/97jd00237>
- Rajesh, T. A., & Ramachandran, S. (2017). Characteristics and source apportionment of black carbon aerosols over an urban site. *Environmental Science and Pollution Research*, 24(9), 8411–8424. <https://doi.org/10.1007/s11356-017-8453-3>
- Sandradewi, J., Prévôt, A. S. H., Szidat, S., Perron, N., Alfarra, M. R., Lanz, V. A., et al. (2008). Using aerosol light absorption measurements for the quantitative

determination of wood burning and traffic emission contributions to particulate matter. *Environmental Science & Technology*, 42(9), 3316–3323. <https://doi.org/10.1021/es702253m>

Satheesh, S. K. and Srinivasan, J.: A method to estimate aerosol radiative forcing from spectral optical depths, *J. Atmos. Sci.*, 63, 1082–1092, <https://doi.org/10.1175/JAS3663.1>, 2006.

Vaishya, A., Singh, P., Rastogi, S., & Babu, S. S. (2017). Aerosol black carbon quantification in the central Indo-Gangetic Plain: Seasonal heterogeneity and source apportionment. *Atmospheric Research*, 185, 13–21. <https://doi.org/10.1016/j.atmosres.2016.10.001>

Xu, H. M., Cao, J. J., Ho, K. F., Ding, H., Han, Y. M., Wang, G. H., Chow, J. C., Watson, J. G., Khol, S. D., Qiang, J., and Li, W. T.: Lead concentrations in fine particulate matter after the phasing out of leaded gasoline in Xi'an, China, *Atmos. Environ.*, 46, 217–224, <https://doi.org/10.1016/j.atmosenv.2011.09.078>, 2012.

Yu, K., Xing, Z., Huang, X., Deng, J., Andersson, A., Fang, W., Gustafsson, Ö., Zhou, J. and Du, K.: Characterizing and sourcing ambient PM<sub>2.5</sub> over key emission regions in China III: Carbon isotope based source apportionment of black carbon, *Atmos. Environ.*, 177, 12–17, <https://doi.org/10.1016/j.atmosenv.2018.01.009>, 2018.

Zhang, D., & Anthes, R. A. (1982). A high-resolution model of the planetary boundary-layer –sensitivity tests and comparisons with sesame-79 data. *Journal of Applied Meteorology*, 21, 1594–1609, [https://doi.org/10.1175/1520-0450\(1982\)021<1594:Ahrmot>2.0.Co;2](https://doi.org/10.1175/1520-0450(1982)021<1594:Ahrmot>2.0.Co;2)

Zhang, T., Cao, J. J., Tie, X. X., Shen, Z. X., Liu, S. X., Ding, H., Han, Y. M., Wang, G. H., Ho, K. F., Qiang, J., and Li, W. T.: Water-soluble ions in atmospheric aerosols measured in Xi'an, China: Seasonal variations and sources, *Atmos. Res.*, 102, 110–119, <https://doi.org/10.1016/j.atmosres.2011.06.014>, 2011.